

Energy Conditions and Stability of Charged Wormholes in $f(R, \mathcal{L}_m)$ Gravity: A Comparative Analysis with Compact Objects

Sagar V. Soni^a, A. C. Khunt^b, Farook Rahaman^c, A. H. Hasmani^a

^a*Department of Mathematics, Sardar Patel University, Vallabh Vidyanagar, 388120, Gujarat, India*

^b*The Gravity Room, Champathal, Amreli, 365601, Gujarat, India*

^c*Department of Mathematics, Jadavpur University, Kolkata, 700032, West Bengal, India*

Abstract

In this paper, we study the energy conditions of charged traversable wormholes in the framework of $f(R, \mathcal{L}_m)$ modified gravity. In the first case, we derive the shape functions (SFs) for two different choices of the charge function \mathcal{E}^2 by considering the Exponential Spheroid (ES) model and analyze the null energy condition (NEC). In the second case, we consider a particular shape function and study its implications for the energy conditions. In both cases, we obtain expressions for energy density and pressure in radial and tangential directions. Our findings show that the radial NEC remains satisfied across a wide range of charge parameters \mathcal{E} consistent with established physical laws. However, the tangential NEC is only sustained in the range $0.1 \leq \mathcal{E} \leq 0.6$; for higher charge values, violations occur, indicating the formation of a throat-like structure necessary for wormhole stability. Additionally, we compare the pressure-density profiles of these charged wormholes with those of compact objects such as neutron stars, revealing distinct variations in matter distribution. This analysis highlights the crucial role of charge and modified gravity in determining the stability and physical characteristics of wormhole structures.

Keywords: Charged Wormhole, $f(R, \mathcal{L}_m)$ gravity, Energy Conditions, ES

Email addresses: sagar.soni7878@gmail.com (Sagar V. Soni), ack.gravity@gmail.com (A. C. Khunt), rahaman@associates.iucaa.in (Farook Rahaman), ah_hasmani@spuvvn.edu (A. H. Hasmani)

1. Introduction

In recent years, hypothetical tunnels connecting distant regions of space-time, known as wormholes, have attracted immense attention due to their profound implications for theoretical physics and cosmology. The exploration of wormholes commenced in 1916 when Flamm [1] presented the mathematical framework for these entities. In response to the instability observed in earlier solutions, Einstein and Rosen [2] proposed the concept of the Einstein–Rosen bridge, which provided a theoretical bridge-like connection within the structure of spacetime. Eventually, it was found that the Einstein-Rosen bridge is not traversable. Notably, the effect of electromagnetic interactions in Einstein’s field equation may be crucial for the creation of wormholes with geons [3, 4]. Morris and Thorne [5] further developed the concept of a traversable wormhole by eliminating the presence of an event horizon.

In the classical theory of relativity, wormhole solutions violate all energy conditions [6]. To address this, the notion of exotic matter was proposed, enabling theoretical traversability, yet the inquiry into their physical existence persists to be unanswered. The pursuit of overcoming the necessity for exotic matter or relieving energy conditions has driven the investigation of alternate gravitational theories.

To avoid reliance on exotic matter, researchers in this area have been attempting a variety of modified theories, notably Einstein-Cartan theory (ECT), teleparallel gravity, $f(Q)$ theory, $f(R)$ theory of gravitation, and many more. In ECT, researchers [7, 8] have obtained the solution of wormhole. The traversable wormholes are explored in $f(Q)$ gravity [9, 10, 11, 12] and $f(R)$ gravity [13, 14, 15, 16, 17, 18, 19, 20].

An expansion of the $f(R)$ theories of gravity, Bertolami et al. [21] investigated the consequences of direct coupling of the scalar curvature R with the matter Lagrangian \mathcal{L}_m , derived the mass-particle equation of motion and found an extra force perpendicular to the four-velocity. Based on this structure, Harko and Lobo [22] used it to extend $f(R)$ gravity to $f(R, \mathcal{L}_m)$ theory, where they derived field equations in the metric formalism and demonstrated that test particle motion is typically non-geodesic because of an additional force perpendicular to the four-velocity. Jaybhaye et. al. [23] have analyzed cosmology within the $f(R, \mathcal{L}_m)$ gravity framework. Researchers have

investigated the geometry of wormholes for various models of the $f(R, \mathcal{L}_m)$ [24, 25, 26, 27]. Recently, Pawde et al. [28] have explored the anisotropic behavior of the universe in $f(R, \mathcal{L}_m)$ gravity.

An alternative way to reduce the necessity of exotic matter is to incorporate charge into the framework [29]. Introducing charged fluids as the source for energy-momentum tensor provides an adequate framework for exploring the interactions among gravitational, electromagnetic, and matter fields. The electromagnetic effects that arise from this approach could eliminate the need for exotic matter to fulfill the requirements of spacetime geometry. Charged fluids are significant as they can reduce repulsive gravitational forces and improve the stability of the wormhole structure. The electric charge of the fluid can generate additional forces that prevent energy condition violations, which is a vital aspect of the possibility of traversable wormholes.

The inclusion of electric charge into traversable wormhole geometries, as demonstrated by Kim and Lee [30], represents a notable expansion of the Morris-Thorne wormhole model. This modification stabilizes wormhole geometry using electromagnetic fields, eliminating the need for exotic matter at the throat. Eiroa and Romero [31] studied the linearized stability of charged thin-shell wormholes and found that higher charge values enhance stability by alleviating constraints on the equation of state. Researchers [32, 33, 34] examined the feasibility of stabilizing a wormhole in ghost scalar field models and scalar-tensor theories of gravity by incorporating electric charge. In $f(T)$ gravity, charged wormhole were studied by Sharif and Rani [35]. Moraes et al. [36] derived solutions for charged wormholes in $f(R, T)$ -extended gravity, demonstrating that charge enhances stability and permits the fulfillment of energy conditions.

The aforementioned literature motivated us to explore traversable wormhole solutions along with a charge in the $f(R, \mathcal{L}_m)$ gravity framework. By selecting a specific model of $f(R, \mathcal{L}_m)$ with the specified Lagrangian \mathcal{L}_m , we will investigate the influence of charge on wormholes in two different ways for constant red-shift function. In the first case, we choose energy density using the ES model and with two various choices of \mathcal{E} , we generate a SF. For the second case we fix the SF and using the equation of state (EoS) parameter, we find out energy and pressures. We also analyze energy conditions and their stability for both cases.

2. Theory of $f(R, \mathcal{L}_m)$ Gravitation

In the framework of different theories of gravitation, one of the approaches is generalizing the action as it describes the influence of field equations. In 2010, Harko and Lobo [22] presented the action principle for the $f(R, \mathcal{L}_m)$ gravity model. This action is defined with the help of matter Lagrangian density \mathcal{L}_m and Ricci scalar R and expressed by

$$S = \int f(R, \mathcal{L}_m) \sqrt{-g} d^4x, \quad (1)$$

where, f is arbitrary function of R and \mathcal{L}_m .

The Ricci scalar R is obtained by the contraction of Ricci tensor R_{ij} , i.e.

$$R = g^{ij} R_{ij}, \quad (2)$$

where,

$$R_{ij} = \partial_k \Gamma_{ij}^k - \partial_j \Gamma_{ki}^k + \Gamma_{ij}^h \Gamma_{hk}^k - \Gamma_{jh}^k \Gamma_{ki}^h, \quad (3)$$

and Γ_{ij}^k represents the components of the Levi-Civita connection given by

$$\Gamma_{ij}^k = \frac{1}{2} g^{kh} \left(\frac{\partial g_{jh}}{\partial x^i} + \frac{\partial g_{hi}}{\partial x^j} - \frac{\partial g_{ij}}{\partial x^h} \right). \quad (4)$$

The field equations for $f(R, \mathcal{L}_m)$ gravity can be obtained by taking the variation of action, as provided in equation (1), with respect to the metric tensor g_{ij} . These equations can be represented as:

$$f_R R_{ij} - \frac{1}{2} (f - f_{\mathcal{L}_m} \mathcal{L}_m) g_{ij} + (g_{ij} \square - \nabla_i \nabla_j) f_R = \frac{1}{2} f_{\mathcal{L}_m} T_{ij}, \quad (5)$$

where, $f_R \equiv \frac{\partial f}{\partial R}$, $f_{\mathcal{L}_m} \equiv \frac{\partial f}{\partial \mathcal{L}_m}$, $\square \equiv \nabla_i \nabla^i$, and T_{ij} is energy-momentum tensor, which can be expressed as:

$$T_{ij} = \frac{-2}{\sqrt{-g}} \frac{\delta(\sqrt{-g} \mathcal{L}_m)}{\delta g^{ij}}. \quad (6)$$

Moreover, the contraction of field equations (5) gives the relation of energy-momentum scalar T , matter Lagrangian \mathcal{L}_m , and Ricci scalar R as:

$$R f_R + 3 \square f_R - 2(f - f_{\mathcal{L}_m} \mathcal{L}_m) = \frac{1}{2} f_{\mathcal{L}_m} T, \quad (7)$$

where, $\square F = \frac{1}{\sqrt{-g}} \partial_i (\sqrt{-g} g^{ij} \partial_j F)$ for any scalar function F .

3. Stable traversable wormholes under the Morris-Thorne space-time

The metric of the Morris-Thorne wormhole, which exhibits spherical symmetry and static behavior, is expressed as follows [5]:

$$ds^2 = -e^{2\Phi(r)} dt^2 + \left(1 - \frac{b(r)}{r}\right)^{-1} dr^2 + r^2 d\theta^2 + r^2 \sin^2 \theta d\phi^2, \quad (8)$$

where, $\Phi(r)$ is red-shift function and $b(r)$ is shape function (SF). This shape function directly affects on the curvature and structure of the throat region. The existence of wormhole solutions requires the satisfaction of the following conditions [5, 6]:

- (i) $b(r_0) = r_0$,
- (ii) For all $r > r_0$, $\frac{b(r)-b'(r)r}{b^2(r)} > 0$, this is called flare-out condition,
- (iii) $b'(r) < 1$,
- (iv) $\frac{b(r)}{r} < 1$ for $r > r_0$,
- (v) $\frac{b(r)}{r} \rightarrow 0$ as $r \rightarrow \infty$,
- (vi) $\Phi(r)$ should be finite everywhere.

Also, note that in (ii), (iii), and (iv), the equality conditions hold at the throat.

For the unit time-like velocity vector $u_i = (e^{-\Phi(r)}, 0, 0, 0)$ and space-like vector $v_i = \left(0, \sqrt{1 - \frac{b(r)}{r}}, 0, 0\right)$, we have taken energy-momentum tensor filled with charged anisotropic fluid, expressed as:

$$T_{ij} = (\rho + p_t)u_i u_j + p_t g_{ij} + (p_r - p_t)v_i v_j + \frac{1}{4\pi} \left[F_{ik} F^k{}_j - \frac{1}{4\pi} g_{ij} F_{kh} F^{kh} \right], \quad (9)$$

where, ρ is the energy density, p_r denotes the radial pressure, and p_t represents the tangential pressure. The F_{ij} is the skew-symmetric electromagnetic field tensor which is defined in terms of 4-potential A_i by

$$F_{ij} = A_{j;i} - A_{i;j}, \quad (10)$$

and it satisfies the Maxwell equations

$$F_{ij;k} + F_{jk;i} + F_{ki;j} = 0, \quad (11)$$

and

$$(F^{ik}\sqrt{-g})_{;k} = 4\pi\sqrt{-g}J^i, \quad (12)$$

where J^i is the current four vector defined by charge density σ as

$$J^i = \sigma(r)u^i. \quad (13)$$

The only non-vanishing components of F_{ij} is F_{01} and the electric field intensity \mathcal{E} is obtained from $\mathcal{E}^2 = -F_{01}F^{01}$, which reduces to

$$\mathcal{E} = \frac{Q(r)}{r^2}. \quad (14)$$

where the Q denotes the total charge. We use geometrized units, in which the electric charge Q is dimensionless and expressed in the same units as length or mass, and also $G = c = 1$.

3.1. Field Equations

For the energy-momentum tensor given in (9), the field equations (5) are written as:

$$\begin{aligned} & \left(1 - \frac{b(r)}{r}\right) \left[\left(\Phi'' + \Phi'^2 + \frac{2\Phi}{r} - \frac{rb'-b}{2r(r-b)}\Phi' \right) F \right. \\ & \quad \left. - \left(\Phi' + \frac{2}{r} - \frac{rb'-b}{2r(r-b)} \right) F' - F'' \right] \\ & + \frac{1}{2}(f - \mathcal{L}_m f \mathcal{L}_m) = \frac{1}{2}f \mathcal{L}_m (\rho + \mathcal{E}^2), \end{aligned} \quad (15)$$

$$\begin{aligned} & \left(1 - \frac{b(r)}{r}\right) \left[\left(-\Phi'' - \Phi'^2 - \frac{rb'-b}{2r(r-b)} \left(\Phi' + \frac{2}{r} \right) \right) F \right. \\ & \quad \left. + \left(\Phi' + \frac{2}{r} - \frac{rb'-b}{2r(r-b)} \right) F' \right] \\ & + \frac{1}{2}(f - \mathcal{L}_m f \mathcal{L}_m) = \frac{1}{2}f \mathcal{L}_m (p_r - \mathcal{E}^2). \end{aligned} \quad (16)$$

$$\begin{aligned} & \left(1 - \frac{b(r)}{r}\right) \left[\left(-\frac{\Phi'}{r} - \frac{rb'+b}{2r^2(r-b)} \right) F \right. \\ & \quad \left. + \left(\Phi' + \frac{2}{r} - \frac{rb'-b}{2r(r-b)} \right) F' - F'' \right] \\ & - \frac{1}{2}(f - \mathcal{L}_m f \mathcal{L}_m) = \frac{1}{2}f \mathcal{L}_m (p_t + \mathcal{E}^2). \end{aligned} \quad (17)$$

4. Solution under specific $f(R, \mathcal{L}_m)$ Model

A general formulation of non-minimal coupling has been presented in the significant work of Harko [37]. Accordingly, a form of $f(R, \mathcal{L}_m)$ is assumed as $f(R, \mathcal{L}_m) = f_1(R) + f_2(R)H(\mathcal{L}_m)$, where, f_1 and f_2 are the function of Ricci scalar R and H is function of matter Lagrangian \mathcal{L}_m . To derive solutions for wormholes, we use a specific minimal form of the $f(R, \mathcal{L}_m)$ function, which is provided by [38, 39]

$$f(R, \mathcal{L}_m) = \frac{R}{2} + \mathcal{L}_m^\alpha, \quad (18)$$

where, α is the free model parameter. The well-known wormhole geometry evolves effortlessly within the classical framework of general relativity by the taking value of $\alpha = 1$.

The Lagrangian density for the specific choice of the $f(R, \mathcal{L}_m)$ model is defined as the function of energy density and is stated to be $\mathcal{L}_m = \rho$, this choice of \mathcal{L}_m is motivated by the work of Harko and other researchers [37, 40, 41].

Therefore, for the specific model of $f(R, \mathcal{L}_m)$ given in (18) with the chosen Lagrangian \mathcal{L}_m , the field equations (15)-(17) reduce to

$$\frac{b'}{r^2} = [(2\alpha - 1)\rho + \alpha\mathcal{E}^2] \rho^{\alpha-1}, \quad (19)$$

$$\frac{2\Phi'}{r} \left(1 - \frac{b}{r}\right) - \frac{b}{r^3} = [\alpha p_r - (\alpha - 1)\rho - \alpha\mathcal{E}^2] \rho^{\alpha-1}, \quad (20)$$

$$\begin{aligned} & [\Phi'' + \Phi'^2 + \frac{\Phi'}{r}] \left(1 - \frac{b}{r}\right) - \left[\Phi' + \frac{1}{r}\right] \left(\frac{rb' - b}{2r^2}\right) \\ & = [\alpha p_t - (\alpha - 1)\rho + \alpha\mathcal{E}^2] \rho^{\alpha-1}. \end{aligned} \quad (21)$$

To solve these field equations, we considered two different cases with a constant red-shift function as follows :

4.1. Case-I

This subsection explores the energy density profile related to the ES model. The ES model is described by the following equation [42]

$$\rho = \rho_0 e^{\frac{-r}{r_s}}, \quad (22)$$

where, ρ_0 , and r_s , are free parameters that represent the central dark matter density and the scale radius. Thus, based on equations (19) and (22), the EC model is governed by the differential equation

$$\frac{b'}{r^2} = \left[(2\alpha - 1)\rho_0 e^{\frac{-r}{r_s}} + \alpha \mathcal{E}^2 \right] \rho_0^{\alpha-1} e^{\frac{-r(\alpha-1)}{r_s}}. \quad (23)$$

To solve the aforementioned differential equation, we consider two distinct scenarios for \mathcal{E}^2 , assuming the value of $r_s = 1$. With the help of the expression (22), we shown the density profile in Fig. 1.

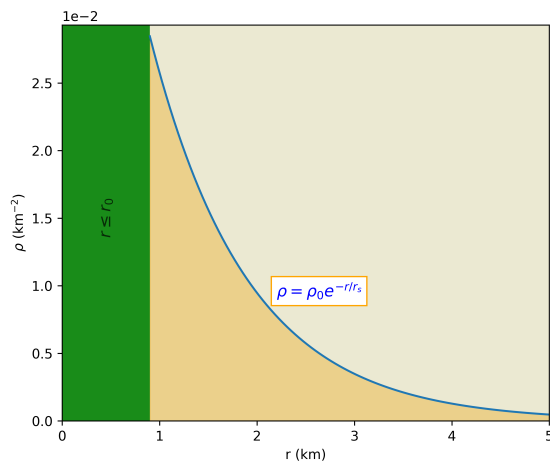


Figure 1: Density ρ plotted against the radial r for the ES-model

The density profile which was computed using Eq. (22) is shown in Fig. 1. The density varies gradually from $3 \times 10^{-3} \text{ km}^{-2}$ to 10^{-1} km^{-2} over the radial domain extending from r_0 to $r \rightarrow \infty$. This behavior corresponds to the expected physical properties of the system, which include a higher density near r_0 that decreases as the radius approaches r_∞ . The profile corresponds to the theoretical predictions for such configurations and allows insight into the spatial distribution of matter within the given framework.

4.1.1. Shape Function-I:-

In this case, we choose $\mathcal{E}^2 = A$, where A is constant. We derive SF as

$$b(r) = \frac{\rho_0^{\alpha-1} e^{\alpha(-r)}}{\alpha^3} \left(- \frac{\alpha^4 A e^r ((\alpha-1)^2 r^2 + 2(\alpha-1)r + 2)}{(\alpha-1)^3} - (2\alpha-1)\rho_0 (\alpha^2 r^2 + 2\alpha r + 2) \right) + C, \quad (24)$$

where C can be obtained by the condition $b(r_0) = r_0$,

$$C = r_0 + \frac{\rho_0^{\alpha-1} e^{\alpha(-r_0)}}{\alpha^3} \left(\frac{\alpha^4 A e^{r_0} ((\alpha-1)^2 r_0^2 + 2(\alpha-1)r_0 + 2)}{(\alpha-1)^3} + (2\alpha-1)\rho_0 (\alpha^2 r_0^2 + 2\alpha r_0 + 2) \right). \quad (25)$$

The flaring-out condition is satisfied if the following constraints hold

$$[(2\alpha-1)\rho_0^\alpha e^{-\alpha r_0} + \alpha A \rho_0^{\alpha-1} e^{-r_0(\alpha-1)}] < \frac{1}{r_0^2}. \quad (26)$$

In the case of GR, $\alpha = 1$, so by above equation we get following inequality

$$\rho_0 < \left[\frac{1}{r_0^2} - A \right] e^{r_0}. \quad (27)$$

Here, we choose $r_0 = 0.9$, $A = 0.5$ and hence, $\rho_0 < 1.8$. We have fixed $\rho_0 = 0.07$ and by inequality (26), we get value of α as $\alpha > 0.72$.

We will use the graphical analysis to determine the feasibility of the wormhole shape function (24) as well as whether it satisfies the necessary requirements for wormhole existence. Figure 2 shows the graphical depiction of $b(r)$, $b(r) - r$, $b'(r)$ and $b(r)/r$. It is crucial to note that for our present investigation, we choose $r_0 = 0.9$, $A = 0.5$, and $\rho_0 = 0.07$, in addition to various changes of parameter α . The graphical representation of $b(r)$, which clearly shows that the condition $b(r_0) = 0$ is satisfied at r_0 , where $r_0 = 0.9$ is the the throat of the wormhole. The asymptotically flat necessity condition for the wormhole SF was satisfied, as shown by the function $b(r)/r \rightarrow 0$ for $r \rightarrow \infty$. The plot indicates that $b'(r) > 0$ is crucial to formation of the wormhole in its present state.

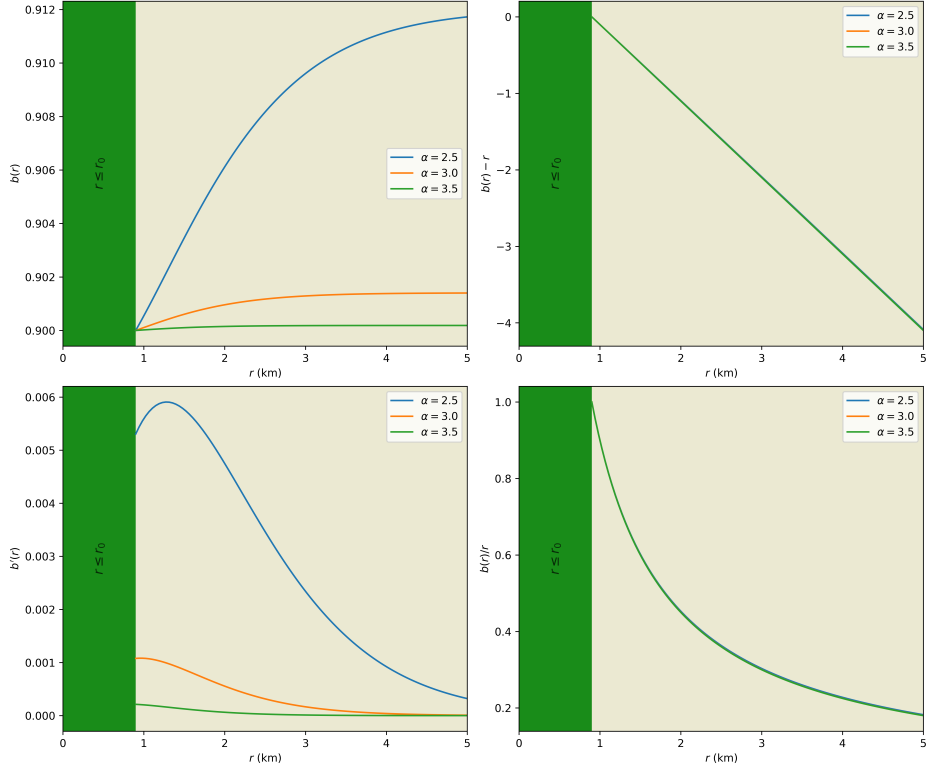


Figure 2: Nature of $b(r)$, throat condition $b(r) < r$, flaring-out condition $b'(r) < 1$, and asymptotic flatness $\lim_{r \rightarrow \infty} \frac{b(r)}{r} = 0$ for $r_0 = 0.9$, $A = 0.5$, $\rho_0 = 0.07$, and $\alpha = \{2.5, 3.0, 3.5\}$.

The radial pressure and tangential pressure can be expressed as

$$\begin{aligned}
 p_r = \frac{1}{\alpha} & \left[(\alpha - 1)\rho_0 e^{-r} + \alpha A + \frac{e^{-r}}{\alpha^3 r^3} \left(\frac{\alpha^4 A e^r ((\alpha - 1)^2 r^2 + 2(\alpha - 1)r + 2)}{(\alpha - 1)^3} \right. \right. \\
 & \left. \left. + (2\alpha - 1)\rho_0 (\alpha^2 r^2 + 2\alpha r + 2) \right) \right. \\
 & \left. - \frac{r_0}{r^3} \rho_0^{1-\alpha} e^{(\alpha-1)r} - \frac{e^{(\alpha-1)r - \alpha r_0}}{\alpha^3 r^3} \left(\frac{\alpha^4 A e^{r_0} ((\alpha - 1)^2 r_0^2 + 2(\alpha - 1)r_0 + 2)}{(\alpha - 1)^3} \right. \right. \\
 & \left. \left. + (2\alpha - 1)\rho_0 (\alpha^2 r_0^2 + 2\alpha r_0 + 2) \right) \right], \tag{28}
 \end{aligned}$$

$$\begin{aligned}
p_t = & \frac{1}{\alpha} \left[(\alpha - 1)\rho_0 e^{-r} - \alpha A \right. \\
& + e^{(\alpha-1)r} \rho_0^{1-\alpha} \left(\frac{1}{2r^3} \left[\frac{\rho_0^{\alpha-1} e^{\alpha(-r)}}{\alpha^3} \left(-\frac{\alpha^4 A e^r ((\alpha - 1)^2 r^2 + 2(\alpha - 1)r + 2)}{(\alpha - 1)^3} \right. \right. \right. \\
& \left. \left. \left. - (2\alpha - 1)\rho_0 (\alpha^2 r^2 + 2\alpha r + 2) \right) \right] + r_0 \right. \\
& \left. + \frac{\rho_0^{\alpha-1} e^{\alpha(-r_0)}}{\alpha^3} \left(\frac{\alpha^4 A e^{r_0} ((\alpha - 1)^2 r_0^2 + 2(\alpha - 1)r_0 + 2)}{(\alpha - 1)^3} \right. \right. \\
& \left. \left. + (2\alpha - 1)\rho_0 (\alpha^2 r_0^2 + 2\alpha r_0 + 2) \right) \right] \\
& \left. - \frac{1}{2r^2} \left[r^2 \rho_0^{\alpha-1} e^{(\alpha-1)(-r)} (\alpha A + (2\alpha - 1)\rho_0 e^{-r}) \right] \right) \Bigg]. \quad (29)
\end{aligned}$$

The graphical illustration of radial pressure and tangential pressure can be

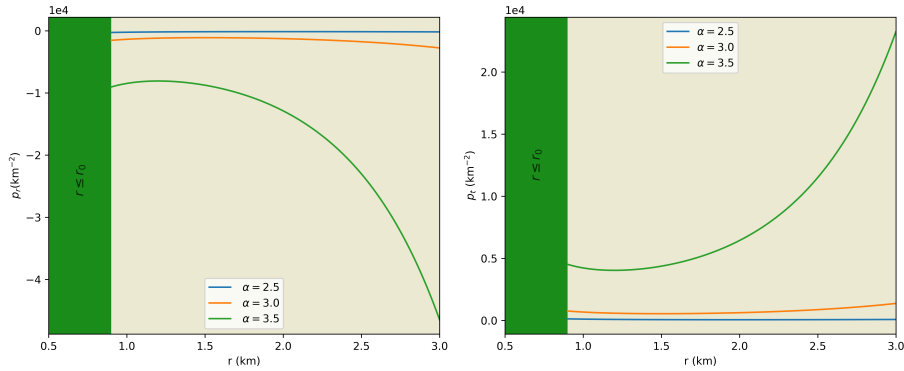


Figure 3: *Left*: Radial pressure p_r and *Right*: Tangential pressure p_t against the radius r for the ES model. The graph shows different curve for the values of α for 2.5, 3.0, and 3.5, with the model parameter set to $A = 0.5$, the density parameter $\rho_0 = 0.07$ and $r_0 = 0.9$ for the charge function $\mathcal{E}^2 = A$.

seen in Fig. 3. It can be noted that radial pressure has negative tendencies whereas tangential pressure is positive and increasing in nature. It is relevant to emphasize here that we choose $r_0 = 0.9$, $A = 0.5$, and $\rho_0 = 0.07$, and for different variations of parameter α as mentioned on the graph.

Within the wormhole structure, particularly in the vicinity of the throat, the energy density ρ shows strictly positive values in its graphical behavior.

Instead of exotic matter, which generally corresponds to negative energy density, this supports the existence of baryonic matter. An anisotropic nature of the matter distribution is further shown by the tangential pressure, p_t , being positive while the radial pressure, p_r , exhibits negative values. Without requiring an escape of energy conditions, the observed pressure anisotropy suggests that the wormhole remains stable by an asymmetric force distribution. We present an anisotropy factor, $\Delta(= p_t - p_r)$, which is shown in Fig. 6a for different values of α .

4.1.2. Shape Function-II:-

The \mathcal{E}^2 selected as $\mathcal{E}^2 = r^2$, we derive SF as

$$b(r) = \frac{\rho_0^{\alpha-1} e^{\alpha(-r)}}{\alpha^3} [2(1-2\alpha)\rho_0 + (1-2\alpha)\alpha^2 \rho_0 r^2 - \frac{\alpha^4 e^r ((\alpha-1)^4 r^4 + 4(\alpha-1)^3 r^3 + 12(\alpha-1)^2 r^2 + 24(\alpha-1)r + 24)}{(\alpha-1)^5} + 2(1-2\alpha)\alpha \rho_0 r] + D, \quad (30)$$

where D is obtained as

$$D = r_0 - \frac{\rho_0^{\alpha-1} e^{\alpha(-r_0)}}{\alpha^3} [2(1-2\alpha)\rho_0 + (1-2\alpha)\alpha^2 \rho_0 r_0^2 - \frac{\alpha^4 e_0^r ((\alpha-1)^4 r^4 + 4(\alpha-1)^3 r^3 + 12(\alpha-1)^2 r_0^2 + 24(\alpha-1)r_0 + 24)}{(\alpha-1)^5} + 2(1-2\alpha)\alpha \rho_0 r_0]. \quad (31)$$

The flaring-out condition is satisfied if the following conditions hold

$$(2\alpha-1)\rho_0^\alpha e^{-\alpha r_0} + \alpha r_0^2 \rho_0^{\alpha-1} e^{-r_0(\alpha-1)} < \frac{1}{r_0^2}. \quad (32)$$

In the case of GR $\alpha = 1$, hence

$$\rho_0 < \left[\frac{1}{r_0^2} - r_0^2 \right] e^{r_0}. \quad (33)$$

Here, we choose $r_0 = 0.9$, and hence $\rho_0 < 1.04$. We have fixed $\rho_0 = 0.07$ and by inequality (32), we get value of α as $\alpha > 0.84$.

The graphical representation of SF with its different conditions given in the Fig. 4. The SF provided in Eq. (30) has a similar graphical behavior

to the previous one, looking after asymptotic flatness with $b(r)/r \rightarrow 0$ as $r \rightarrow \infty$ and satisfies $b(r_0) = 0$ at $r_0 = 0.9$. Additionally, wormhole formation is ensured by upholding the requirement $b'(r) > 0$. Even if the general trends are in agreement, little changes in parameters might result in somewhat different geometrical characteristics.

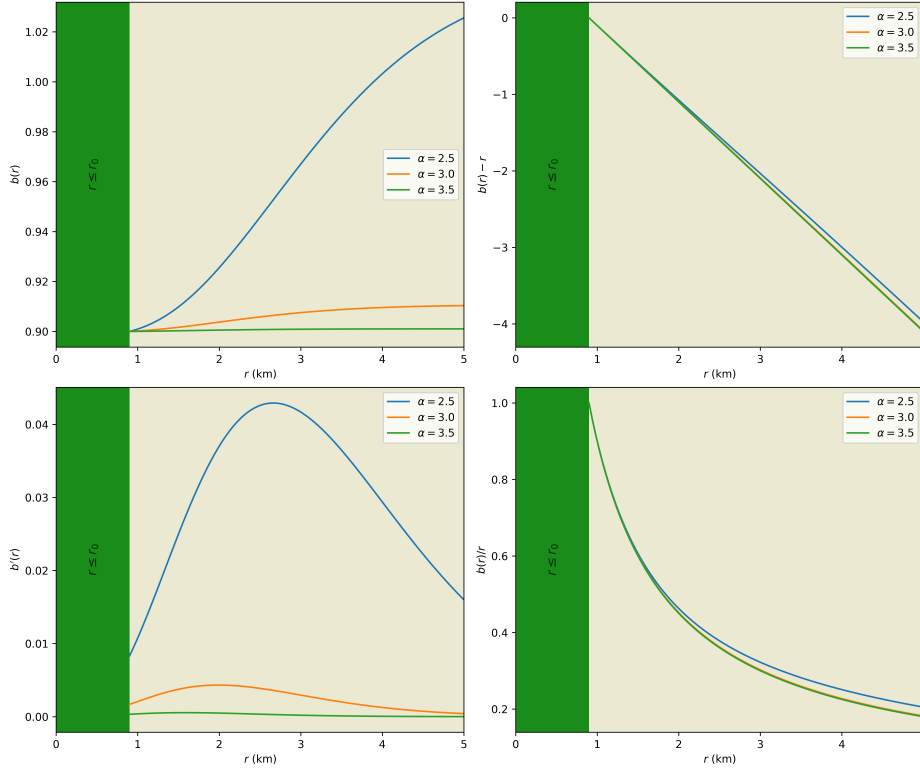


Figure 4: Nature of $b(r)$, throat condition $b(r) < r$, flaring-out condition $b'(r) < 1$, and asymptotic flatness $\lim_{r \rightarrow \infty} \frac{b(r)}{r} = 0$ for $r_0 = 0.9$, $\rho_0 = 0.07$, and $\alpha = \{2.5, 3.0, 3.5\}$.

The radial pressure and tangential pressure are now

$$\begin{aligned}
\alpha p_r = & (\alpha - 1)\rho_0 e^{-r} + \alpha r^2 - \frac{\rho_0^{(1-\alpha)} e^{(\alpha-1)r}}{r^3} \left(\frac{\rho_0^{\alpha-1} e^{\alpha(-r)}}{\alpha^3} [2(1-2\alpha)\rho_0 + (1-2\alpha)\alpha^2 \rho_0 r^2 \right. \\
& - \frac{\alpha^4 e^r ((\alpha-1)^4 r^4 + 4(\alpha-1)^3 r^3 + 12(\alpha-1)^2 r^2 + 24(\alpha-1)r + 24)}{(\alpha-1)^5} \\
& + 2(1-2\alpha)\alpha \rho_0 r] + r_0 - \frac{\rho_0^{\alpha-1} e^{\alpha(-r_0)}}{\alpha^3} [2(1-2\alpha)\rho_0 + (1-2\alpha)\alpha^2 \rho_0 r_0^2 \\
& - \frac{\alpha^4 e_0^r ((\alpha-1)^4 r^4 + 4(\alpha-1)^3 r_0^3 + 12(\alpha-1)^2 r_0^2 + 24(\alpha-1)r_0 + 24)}{(\alpha-1)^5} \\
& \left. + 2(1-2\alpha)\alpha \rho_0 r_0] \right), \tag{34}
\end{aligned}$$

$$\begin{aligned}
\alpha p_t = & (\alpha - 1)\rho_0 e^{-r} - \alpha r^2 + \rho_0^{(1-\alpha)} e^{(\alpha-1)r} \left[\frac{1}{2r^3} \left(\frac{\rho_0^{\alpha-1} e^{\alpha(-r)}}{\alpha^3} [2(1-2\alpha)\rho_0 + (1-2\alpha)\alpha^2 \rho_0 r^2 \right. \right. \\
& - \frac{\alpha^4 e^r ((\alpha-1)^4 r^4 + 4(\alpha-1)^3 r^3 + 12(\alpha-1)^2 r^2 + 24(\alpha-1)r + 24)}{(\alpha-1)^5} \\
& + 2(1-2\alpha)\alpha \rho_0 r] + r_0 - \frac{\rho_0^{\alpha-1} e^{\alpha(-r_0)}}{\alpha^3} [2(1-2\alpha)\rho_0 + (1-2\alpha)\alpha^2 \rho_0 r_0^2 \\
& - \frac{\alpha^4 e_0^r ((\alpha-1)^4 r^4 + 4(\alpha-1)^3 r_0^3 + 12(\alpha-1)^2 r_0^2 + 24(\alpha-1)r_0 + 24)}{(\alpha-1)^5} \\
& \left. \left. + 2(1-2\alpha)\alpha \rho_0 r_0] \right) - \frac{1}{2r^2} \left(r^2 (2\alpha-1) \rho_0^\alpha e^{-\alpha r} + \alpha r^2 \rho_0^{\alpha-1} e^{-r(\alpha-1)} \right) \right]. \tag{35}
\end{aligned}$$

For the SF in Eq. (30), the radial pressure p_r stays positive and evolves with the radial coordinate, whereas the tangential pressure p_t is negative and falls with radius. This behavior differs from the prior SF, when p_r was negative and p_t was positive and increasing. The positive p_r in this situation suggests a different force balance, which may affect the energy condition

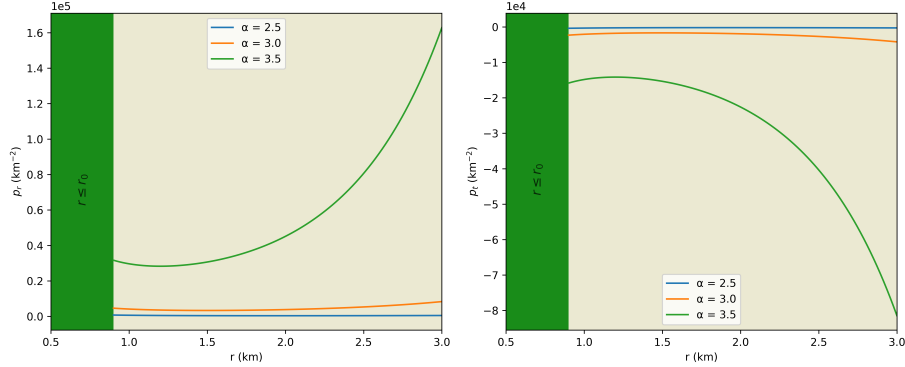


Figure 5: *Left*: Radial pressure p_r and *Right*: Tangential pressure p_t against the radius r for the ES model. The graph shows different curve for the values of α for 2.5, 3.0, and 3.5., the density parameter $\rho_0 = 0.07$ and $r_0 = 0.9$ for the charge function $\mathcal{E}^2 = r^2$.

necessities. However, the anisotropic stress distribution supports the general stability of the wormhole structure.

Figs. 6 show the anisotropy profile $\Delta = p_t - p_r$ for both SFs. SF-1 has a negative p_r and a positive p_t . This leads to a positive anisotropy parameter that increases with radial coordinate. The anisotropy ranges from 10^2 to 10^4 km^{-2} , showing a significant tangential stress contribution.

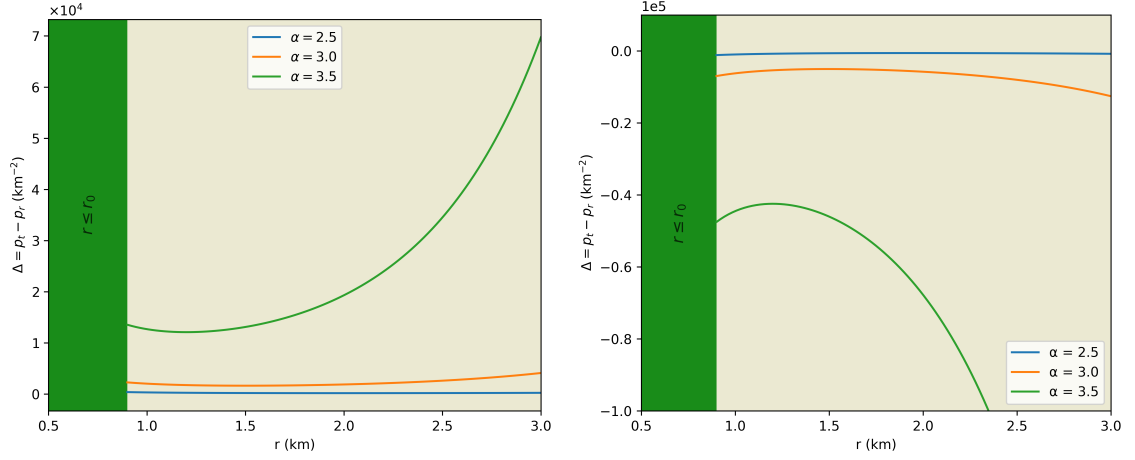
On the other hand, for SF-2, where the p_r is positive and the p_t is negative, the anisotropy parameter is negative throughout the domain, as shown in Figure 6b. The anisotropy ranges from -10^2 to -10^4 km^{-2} , showing an inverted stress distribution compared to SF-1.

An outward-directed anisotropy ($\Delta > 0$) is usually favorable for the existence of a traversable wormhole because it provides the required repulsive force to overcome gravity collapse while maintaining the wormhole throat. A typical feature of wormhole physics is the needed violation of the NEC, which can be made possible by a positive anisotropy, where $p_t > p_r$. On the other hand, a negative anisotropy ($\Delta < 0$) indicates a radially dominating pressure, which could not obviously allow a traversable wormhole structure but might result in another type of stable exotic matter structure.

4.2. Case II

In this study, we explore the wormhole model by varying the values of the charge parameter while considering the EoS parameter with a fixed SF.

Theoretically, the EoS parameter ω is an essential parameter, especially



(a) Anisotropy variation for the SF-I

(b) Anisotropy variation for the SF-II

Figure 6: (a) Radial variation of anisotropy parameter Δ for the SF-I and (b) Radial variation of anisotropy parameter Δ for the SF-II with the parameters set to $A = 0.5$, $r_0 = 0.9$, $\rho_0 = 0.07$, and different values of α 2.5, 3.0, 3.5.

when examining gravitational theories, cosmology, and astrophysics [43]. To examine energy conditions for the wormhole, we have considered linear barotropic EoS. It establishes a relationship between the radial pressure p_r and the energy density ρ of given matter as

$$p_r = \omega \rho. \quad (36)$$

For a particular choice of SF taken as $b(r) = r e^{1 - \frac{r}{r_0}}$ with constant redshift function and by considering EoS parameter given in (36), the field equations (19)-(21) can be written as

$$\rho = \frac{2\alpha \mathcal{E}^2}{[(\omega - 1)\alpha + 1] \frac{r}{r_0} - (\omega + 1)\alpha}, \quad (37)$$

$$p_r = \frac{2\alpha \omega \mathcal{E}^2}{[(\omega - 1)\alpha + 1] \frac{r}{r_0} - (\omega + 1)\alpha}, \quad (38)$$

$$p_t = \frac{1}{\alpha} \left[\frac{e^{1-\frac{r}{r_0}}}{2rr_0} \left\{ \frac{2\alpha\omega\mathcal{E}^2}{[(\omega-1)\alpha+1]\frac{r}{r_0} - (\omega+1)\alpha} \right\}^{1-\alpha} + (\alpha-1) \frac{2\alpha\mathcal{E}^2}{[(\omega-1)\alpha+1]\frac{r}{r_0} - (\omega+1)\alpha} - \alpha\mathcal{E}^2 \right]. \quad (39)$$

Eqs. (37), (38), and (39) are the expressions for density, radial pressure, and tangential pressure, respectively.

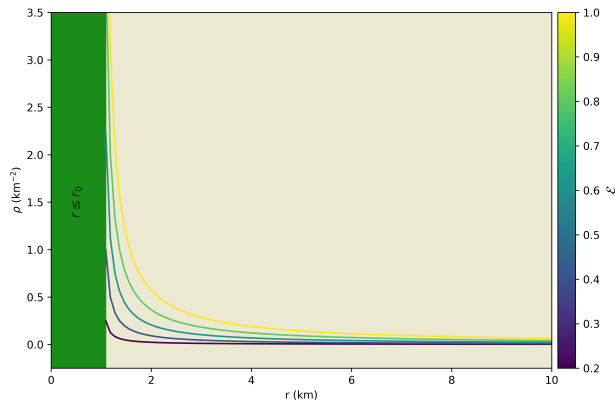


Figure 7: Density ρ plotted against the radius r for a charged wormhole. The plot shows different curves for electric charge values \mathcal{E} ranging from 0 to 1, with the model parameters set to $\alpha = 0.5$, EoS parameter $\omega = 2.5$, and throat radius $r_0 = 1$.

Fig. 7, presents the density ρ as a function of the radial coordinate r , computed via Eq.(37) from the modified $f(R, \mathcal{L}_m)$ gravity. The model parameter is set at $\alpha = 0.5$, the EoS parameter at $\omega = 2.5$, and the electric charge \mathcal{E} ranges from 0 to 1. The plot shows the density ρ is greatest near the wormhole throat and progressively lowers as r rises. In addition, we notice that greater magnitudes of \mathcal{E} are correlated with increased densities around the throat. As the magnitude of the charge decreases the density curve accordingly lowers, emphasizing the apparent connection between electric charge and density distribution in the wormhole model.

In this study of wormholes adopting the framework of $f(R, \mathcal{L}_m)$ gravity, we check out the behavior of tangential and radial pressures as functions of the radial coordinate r , taking into account a particular range of charge

values \mathcal{E} . The results show clear patterns in the pressure profiles based on the charge magnitude, as shown in Figs. (8a) and (8b).

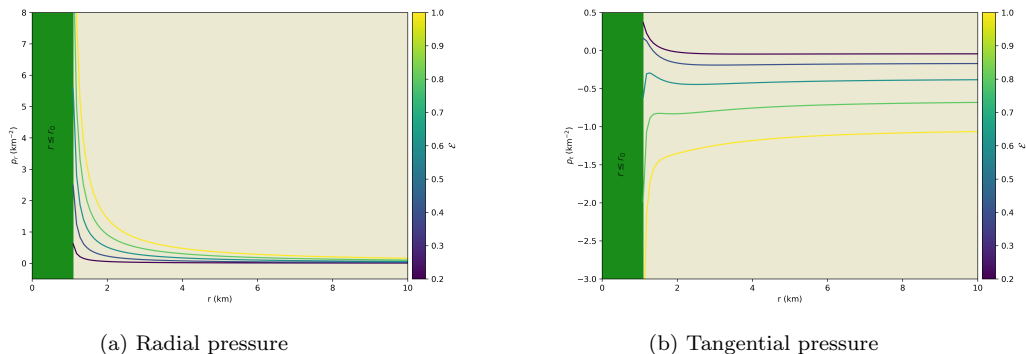


Figure 8: (a) Radial pressure p_r and (b) tangential pressure p_t plotted against the radius r for a charged wormhole. The graphs show different curves for electric charge values \mathcal{E} ranging from 0 to 1, with the model parameters set to $\alpha = 0.5$, EoS parameter $\omega = 2.5$, and throat radius $r_0 = 1$.

The profile for the p_r shows positive values across the whole range that is taken into consideration, including the exterior region of the wormhole throat. However, for a high \mathcal{E} , the radial pressure reaches its highest value, demonstrating that stronger charge leads to increased radial pressure. The p_r continuously falls with increasing radial distance from the throat, pointing to the anticipated reduction of the electromagnetic effect with distance. While in the under consideration range, the wormhole structure seems to be stable under the effects of the radial forces, as shown by the positive radial pressure throughout all \mathcal{E} ranges.

The tangential pressure, p_t on the other hand, exhibits more intricate behavior. Although it is lower in magnitude than the radial pressure p_r , the tangential pressure p_t remain positive across the charge range of $\mathcal{E} = 0.1$ to 0.35 . This shows a decreased p_t on the wormhole structure in the slight charge range. For the charge amount over $\mathcal{E} \approx 0.35$, p_t becomes negative, suggesting a tension-like action rather than compression. The tendency toward negative values means the introduction of anisotropic pressure ($\Delta = p_t - p_r \neq 0$) by higher charges results in a decrease of p_t , which could suggest an instability in the direction of forces for larger charge magnitudes.

Fig. 9 shows the anisotropy profile Δ as a function of r , to show the interplay between pressures p_r and p_t . The pressure p_r is regularly larger

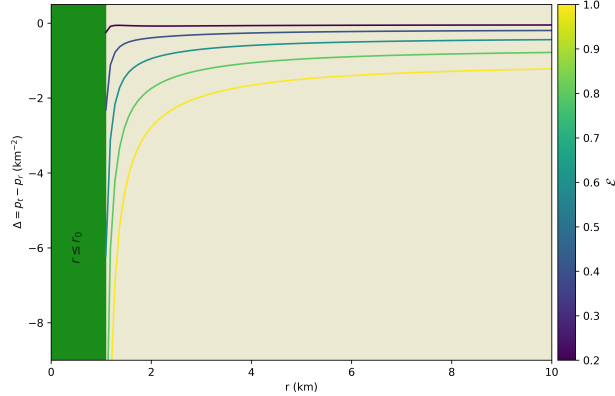


Figure 9: Radial variation of anisotropy parameter Δ for $\alpha = 0.5$, $\omega = 2.5$, and $r_0 = 1$.

than p_t over the radial coordinate range. The structure provides a significant amount of p_r in the region where $\Delta < 0$, signifying larger p_r that maintain the wormhole's structure, which is closest to the throat. This is crucial to keep the wormhole in its present shape to avoid any collapse driven on by the gravitational forces playing in a radial direction.

In a more plausible way, comparing this energy profile with the EoS of a neutron star-like compact object could provide a fair comparison between exotic matter and energy scale. Recently, many researchers investigated different kinds of exotic matter within the framework of highly gravitating compact objects; such exotic matter plays a crucial role in the anatomy of neutron stars and quark star-like objects.

In Case II, the pressure-density profile shows that the matter density varies between around 0.1 and 10 km^{-2} , whereas the radial pressure varies within $1 - 16 \text{ km}^{-2}$. However, in Case I, the pressure fluctuates within a much larger range of approximately $10^3 - 10^4 \text{ km}^{-2}$, while the density varies between about $10^{-3} - 10^{-2} \text{ km}^{-2}$. In compare to Case II, this shows that the pressure-density factors of different wormhole solutions can differ significantly, which at first may result in varying stability criteria and physical interpretations under strong gravitational fields. A few different EoS are compared in detail in Table 1, including those for wormhole configurations, geometrically obtained models, and neutron stars. In accordance with current understandings of nuclear matter, the first two EoS (SLy and SQM) are neutron stars. The density of these neutron-like compact stars ranges

from around $10^{-28} - 10^{-24} \text{ km}^{-2}$ (in geometric units)¹, whereas the pressure varies between $\sim 10^{-10} - 10^{-2} \text{ km}^{-2}$. The pressure-density relations are determined by spacetime geometry itself, as pointed out by the two geometrically obtained EoS (TRV and SNJR), which were calculated directly from Einstein's equations [44, 45].

On the other hand, the wormhole EoS serves very differently in each case. In Case II, the density typically ranges between 1 km^{-2} and 6 km^{-2} , and the pressure varies between $1 - 16 \text{ km}^{-2}$. On the other hand, for Case I, the density typically ranges from 10^{-3} km^{-2} to 10^{-2} km^{-2} , whereas the pressure varies between roughly 10^3 km^{-2} to 10^4 km^{-2} . This is far more than that of typical neutron stars, demonstrating that wormholes as well as other unusual compact objects are impacted by gravitational fields that are far stronger. Wormholes are controlled by the curvature of spacetime itself, in comparison to neutron stars, which are made of nuclear matter.

This analogy emphasizes the important difference between exotic objects like wormholes and compact stars like neutron stars. The pressure-density profile of wormholes is determined by strong gravitational draws rather than material properties. This observation offers significant insight concerning how to determine an appropriate geometric model for this sort of object. Since spacetime is a feature of geometry at its most fundamental, the most effective approach to understanding such strange objects is through gravity theory. We still are unaware of exactly what these objects are made of on their interiors. In addition, it further highlights the significance of further investigation to better understand such strong gravity objects and how different geometries influence their characteristics.

¹The density and pressure in geometric units (km^{-2}) can be converted to CGS units as follows:

$$\rho_{\text{cgs}} = \rho_{\text{geom}} \frac{c^2}{G}, \quad p_{\text{cgs}} = p_{\text{geom}} \frac{c^2}{G},$$

where $G = 6.67430 \times 10^{-8} \text{ cm}^3 \text{ g}^{-1} \text{ s}^{-2}$ and $c = 3 \times 10^{10} \text{ cm/s}$. :

$$\rho_{\text{geom}} = \rho_{\text{cgs}} \frac{G}{c^2}, \quad p_{\text{geom}} = p_{\text{cgs}} \frac{G}{c^2}$$

Compact stars

EoS	EoS type/model	ρ (km ⁻²)	p (km ⁻²)
SLy [46]	Nuclear matter	$\sim 10^{-28} - 10^{-24}$	$\sim 10^{-17} - 10^{-3}$
SQM [47]	Quark matter	$\sim 10^{-26} - 10^{-24}$	$\sim 10^{-4} - 10^{-3}$
TRV [44, 45]	Geometrical	$\sim 10^{-23} - 10^{-25}$	$\sim 10^{-8} - 10^{-2}$
SNJR [44, 45]	Geometrical	$\sim 10^{-25} - 10^{-24}$	$\sim 10^{-8} - 10^{-5}$
Wormholes			
Solanki et al.[48]	$f(R, \mathcal{L}_m)$	$\sim 1 - 8$	$\sim 10^{-2} - 10^{-1}$
Present study	$f(R, \mathcal{L}_m)$ gravity (case I)	$\sim 10^{-3} - 10^{-2}$	$\sim 10^3 - 10^4$
	$f(R, \mathcal{L}_m)$ gravity (case II)	$\sim 1 - 6$	$\sim 1 - 16$

Table 1: Comparison of EoS for compact stars and wormholes, showing the type of EoS, density (ρ), and pressure (p) ranges. The data includes nuclear matter (SLy and SQM), geometrically derived models (TRV and SNJR), and wormhole configurations (Solanki et al.[48] and the present study). All values are expressed in geometric units (km⁻²).

5. Energy condition

We study wormhole energy conditions determining if they follow conventional physical laws, such as the null energy condition, and to examine whether they are feasible to exist in the context of modified gravitational theories.

The energy-condition relations for traversable wormholes can be constructed based on their anisotropic distribution of matter [5, 49].

1. Null Energy Condition: $\rho + p_r \geq 0$, $\rho + p_t \geq 0$,
2. Weak Energy Condition: $\rho \geq 0$, $\rho + p_r \geq 0$, $\rho + p_t \geq 0$,
3. Dominant Energy Condition: $\rho \geq 0$, $\rho \pm p_r \geq 0$, $\rho \pm p_t \geq 0$,
4. Strong Energy Condition: $\rho + p_r \geq 0$, $\rho + p_t \geq 0$, $\rho + p_r + 2p_t \geq 0$

The investigation on the energy conditions in $f(R, \mathcal{L}_m)$ gravity is elaborated in [50]. In the present study, we only present the NEC for the both cases, which is graphically represented in this section.

For each case, the NEC behaviour is shown for the tangential (NEC_t) and radial (NEC_r) components. For case-I, Fig. 10 and 11 show NEC_r and NEC_t , respectively, for two different charge function choices. Fig. 12, on the other hand, shows the NEC_r and NEC_t for case-II.

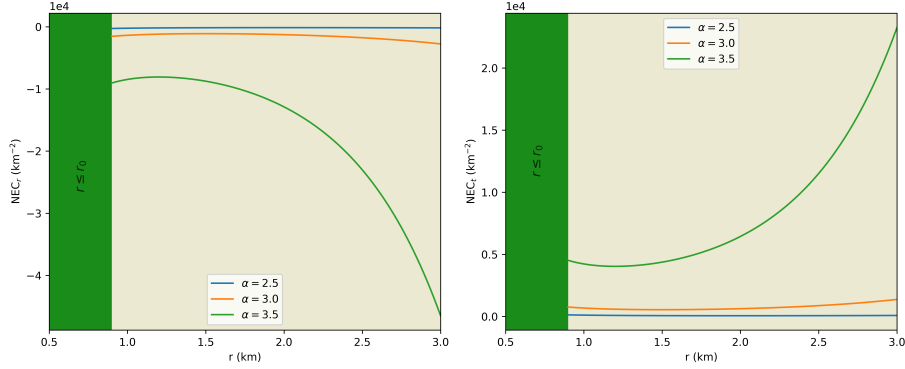


Figure 10: *Left*: Radial NEC and *Right*: Tangential NEC for SF-I

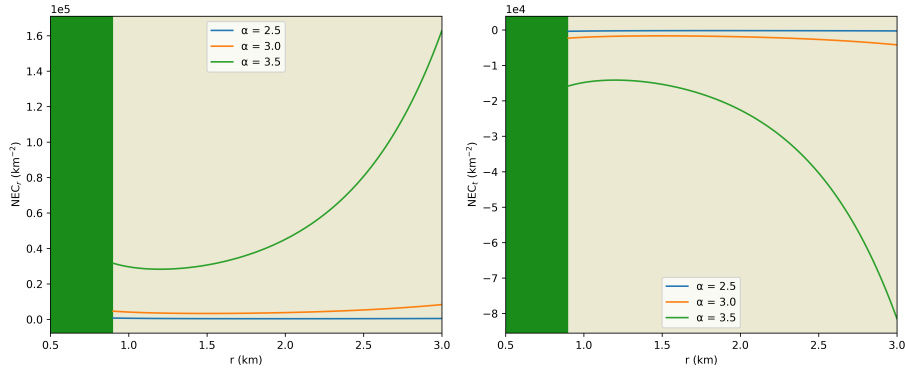


Figure 11: *Left*: Radial NEC and *Right*: Tangential NEC for SF-II

We present the NEC for the ES density model, taking into consideration two distinct charge function choices, for both the NEC_r and NEC_t components. The NEC is shown for the charge function $\mathcal{E}^2 = A$ in Fig. 10, and for $\mathcal{E}^2 = r^2$ in Fig. 11.

The NEC_r for $\mathcal{E}^2 = A$ fails to fulfill the NEC in the radial direction as it violates the $\rho + p_r \geq 0$ condition. However, NEC_t remains its positive contribution by following the NEC requirements. As a result, NEC_t exhibits a negative curve, which violates the NEC in the tangential direction, whereas NEC_r shows a positive nature, satisfying the NEC for $\mathcal{E}^2 = r^2$.

As long as the \mathcal{E} persists greater than a value of zero, the radial NEC_r is satisfied. This is consistent from the r_0 to the maximum radius (r_{max}). In context, it indicates that the p_r consistently supports the energy condition

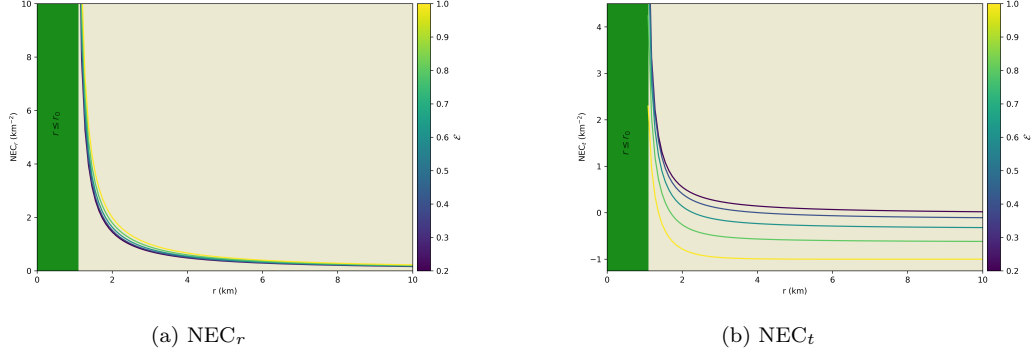


Figure 12: Null energy condition (NEC) for radial and tangential pressures for different values of \mathcal{E} . (a) NEC for radial pressure, which remains satisfied across the range. (b) NEC for tangential pressure, showing satisfaction within $0.1 \leq \epsilon \leq 0.6$ and violation for $\mathcal{E} > 0.6$.

when a charge is involved.

On the other hand, NEC_t shows a more restricted behavior. For \mathcal{E} in the range $0.1 \leq \mathcal{E} \leq 0.6$, the NEC_t is fulfilled, validating the energy condition within this interval. However, when the charge exceeds $\mathcal{E} > 0.6$, the NEC_t is violated. Variations in tangential pressure cause this violation, leading to the formation of a throat-like environment that is crucial to maintaining the wormhole-like structure.

6. Conclusion

In the context of $f(R, \mathcal{L}_m)$ modified gravity, we investigated the possible existence of charged traversable wormholes. By taking energy momentum tensor as charged fluid, the field equations for $f(R, \mathcal{L}_m)$ gravity have been derived. For this study, the minimal coupling model $f(R, \mathcal{L}_m) = \frac{R}{2} + \mathcal{L}_m^\alpha$ has been considered. To simplify the expression of density and pressures, we have employed the EoS parameter along with specific shape and redshift functions.

We have constructed two different shape functions based on the choices $\mathcal{E}^2 = A$ and $\mathcal{E}^2 = r^2$ using the ES model. For SF-I, Fig. 10 shows that the NEC_r is not satisfied, while the NEC_t holds for all values of α . On the other hand, for SF-II, Fig. 11 indicates that NEC_t is not satisfied, whereas NEC_r holds for all values of α . Therefore, for both shape functions (SF-I and SF-II), the NEC conditions are not fully satisfied.

We have obtained the expression of energy conditions for the particular choice of SF $b(r) = re^{1-\frac{r}{r_0}}$. The existence of wormholes requires the fulfillment of the NEC. From Fig. (7), it can be observed that the energy density is positive throughout spacetime. Also, by (12a), it can be seen that radial NEC is satisfied for all the values of $\mathcal{E} > 0$. However, as we can see from the Fig. (12b), tangential NEC is valid only for the range $0.1 \leq \mathcal{E} \leq 0.6$. Therefore, NEC is valid only for $0.1 \leq \mathcal{E} \leq 0.6$ and hence for $\mathcal{E} > 0.6$ results into existence of exotic matter.

Moreover, the significance of incorporating modified gravity theories into our understanding of compact objects is shown by the significant differences in the energy profiles of charged wormholes and neutron stars. Neutron stars are well described by general relativity when matter is distributed in a standard way. However, charged wormholes in modified gravity models question these assumptions and suggest that exotic matter distributions may be required to sustain such structures. These different energy requirements show that general relativity can't fully explain non-standard events. These findings also demonstrate the potential of modified gravity theories to provide a more comprehensive framework for analyzing the physical properties of exotic objects such as wormholes.

Acknowledgements

SVS is thankful to the CSIR, India for providing financial support under CSIR Senior Research Fellowship (09/157(0059)/2021-EMR-I), and also thankful to IUCAA, Pune for the facilities and hospitality provided to him where the part of work was carried out.

References

- [1] L. Flamm, Contributions to Einstein's theory of gravitation, Hirzel, 1916.
- [2] A. Einstein, N. Rosen, The Particle Problem in the General Theory of Relativity, Phys. Rev. 48 (1935) 73–77. [doi:10.1103/PhysRev.48.73](https://doi.org/10.1103/PhysRev.48.73).
- [3] J. A. Wheeler, Geons, Phys. Rev. 97 (1955) 511–536. [doi:10.1103/PhysRev.97.511](https://doi.org/10.1103/PhysRev.97.511).

- [4] C. W. Misner, J. A. Wheeler, Classical physics as geometry, *Annals of Physics* 2 (6) (1957) 525–603. doi:[https://doi.org/10.1016/0003-4916\(57\)90049-0](https://doi.org/10.1016/0003-4916(57)90049-0).
- [5] M. S. Morris, K. S. Thorne, Wormholes in spacetime and their use for interstellar travel: A tool for teaching general relativity, *American Journal of Physics* 56 (5) (1988) 395–412. doi:<https://doi.org/10.1119/1.15620>.
- [6] M. Visser, *Lorentzian Wormholes. From Einstein to Hawking*, Woodbury (1995).
- [7] K. A. Bronnikov, A. M. Galiakhmetov, Wormholes without exotic matter in Einstein–Cartan theory, *Gravitation and Cosmology* 21 (2015) 283–288. doi:<https://doi.org/10.1134/S0202289315040027>.
- [8] Soni, Sagar V. and Khunt, A. C. and Hasmani, A. H., A study of Morris–Thorne wormhole in Einstein–Cartan theory, *International Journal of Geometric Methods in Modern Physics* 21 (06) (2024) 2450115. doi:[10.1142/S0219887824501159](https://doi.org/10.1142/S0219887824501159).
- [9] A. Banerjee, A. Pradhan, T. Tangphati, F. Rahaman, Wormhole geometries in $f(Q)$ gravity and the energy conditions, *The European Physical Journal C* 81 (2021) 1031. doi:[10.1140/epjc/s10052-021-09854-7](https://doi.org/10.1140/epjc/s10052-021-09854-7).
- [10] F. Parsaei, S. Rastgoo, P. K. Sahoo, Wormhole in $f(Q)$ gravity, *The European Physical Journal Plus* 137 (2022) 1083. doi:[10.1140/epjp/s13360-022-03298-y](https://doi.org/10.1140/epjp/s13360-022-03298-y).
- [11] S. Chaudhary, S. Maurya, J. Kumar, S. Ray, Stability analysis of wormhole solutions in $f(Q)$ gravity utilizing Karmarkar condition with radial dependent redshift function, *Astroparticle Physics* 162 (2024) 103002. doi:<https://doi.org/10.1016/j.astropartphys.2024.103002>.
- [12] M. Jan, A. Ashraf, A. Basit, A. Caliskan, E. Güdekli, Traversable Wormhole in $f(Q)$ Gravity Using Conformal Symmetry, *Symmetry* 15 (4) (2023). doi:[10.3390/sym15040859](https://doi.org/10.3390/sym15040859).
- [13] F. S. N. Lobo, M. A. Oliveira, Wormhole geometries in $f(R)$ modified theories of gravity, *Physical Review D* 80 (10) (2009) 104012. doi:[10.1103/PhysRevD.80.104012](https://doi.org/10.1103/PhysRevD.80.104012).

- [14] K. A. Bronnikov, A. A. Starobinsky, No static spherically symmetric wormholes in scalar-tensor and $f(R)$ gravity, JETP Letters 85 (1) (2007) 1–5. doi:[10.1134/S0021364007010018](https://doi.org/10.1134/S0021364007010018).
- [15] P. Pavlovic, M. Sossich, Wormholes in viable $f(R)$ modified theories of gravity and Weak Energy Condition, European Physical Journal C 75 (3) (2015) 117. doi:[10.1140/epjc/s10052-015-3347-3](https://doi.org/10.1140/epjc/s10052-015-3347-3).
- [16] S. H. Mazharimousavi, M. Halilsoy, Wormhole solutions in $f(R)$ gravity satisfying energy conditions, Modern Physics Letters A 31 (16) (2016) 1650093. doi:[10.1142/S0217732316500938](https://doi.org/10.1142/S0217732316500938).
- [17] S. Bahamonde, U. Camci, Exact traversable wormhole solutions in $f(R)$ gravity by Noether symmetry approach, Symmetry 10 (12) (2018) 774. doi:[10.3390/sym10120774](https://doi.org/10.3390/sym10120774).
- [18] P. H. R. S. Moraes, P. K. Sahoo, Modeling wormholes in $f(R, T)$ gravity, Physical Review D 96 (4) (2017) 044038. doi:[10.1103/PhysRevD.96.044038](https://doi.org/10.1103/PhysRevD.96.044038).
- [19] N. Godani, G. C. Samanta, Traversable wormholes and energy conditions with two different shape functions in $f(R)$ gravity, International Journal of Modern Physics D 28 (2) (2019) 1950039. doi:[10.1142/S0218271819500398](https://doi.org/10.1142/S0218271819500398).
- [20] S. Capozziello, A. S. Ditta, E. N. Saridakis, K. Yin, Traversable Wormholes with Vanishing Sound Speed in $f(R)$ Gravity, European Physical Journal C 81 (2) (2021) 134. doi:[10.1140/epjc/s10052-021-08996-y](https://doi.org/10.1140/epjc/s10052-021-08996-y).
- [21] O. Bertolami, C. G. Böhrer, T. Harko, F. S. N. Lobo, Extra force in $f(R)$ modified theories of gravity, Phys. Rev. D 75 (2007) 104016. doi:[10.1103/PhysRevD.75.104016](https://doi.org/10.1103/PhysRevD.75.104016).
- [22] T. Harko, F. S. N. Lobo, $f(R, L_m)$ gravity, The European Physical Journal C 70 (2010) 373–379. doi:<https://doi.org/10.1140/epjc/s10052-010-1467-3>.
- [23] L. V. Jaybhaye, S. Bhattacharjee, P. Sahoo, Baryogenesis in $f(R, L_m)$ gravity, Physics of the Dark Universe 40 (2023) 101223. doi:<https://doi.org/10.1016/j.dark.2023.101223>.

- [24] N. Kavya, V. Venkatesha, G. Mustafa, P. Sahoo, S. Divya Rashmi, Static traversable wormhole solutions in $f(R, \mathcal{L}_m)$ gravity, Chinese Journal of Physics 84 (2023) 1–11. doi:<https://doi.org/10.1016/j.cjph.2023.05.002>.
- [25] R. Solanki, Z. Hassan, P. Sahoo, Wormhole solutions in $f(R, L_m)$ gravity, Chinese Journal of Physics 85 (2023) 74–88. doi:<https://doi.org/10.1016/j.cjph.2023.06.005>.
- [26] T. Naseer, M. Sharif, A. Fatima, S. Manzoor, Constructing traversable wormhole solutions in $f(R, L_m)$ theory, Chinese Journal of Physics 86 (2023) 350–360. doi:<https://doi.org/10.1016/j.cjph.2023.10.032>.
- [27] L. V. Jaybhaye, M. Tayde, P. K. Sahoo, Wormhole solutions under the effect of dark matter in $f(R, L_m)$ gravity, Communications in Theoretical Physics 76 (5) (2024) 055402. doi:[10.1088/1572-9494/ad3746](https://doi.org/10.1088/1572-9494/ad3746).
- [28] J. Pawde, R. Mapari, V. Patil, et al., Anisotropic behavior of universe in $f(R, L_m)$ gravity with varying deceleration parameter, European Physical Journal C 84 (2024) 320. doi:[10.1140/epjc/s10052-024-12646-4](https://doi.org/10.1140/epjc/s10052-024-12646-4).
- [29] P. H. R. S. Moraes, W. de Paula, R. A. C. Correa, Charged wormholes in $f(R, T)$ extended theory of gravity, Int. J. Mod. Phys. D 28 (08) (2019) 1950098. doi:[10.1142/S0218271819500986](https://doi.org/10.1142/S0218271819500986).
- [30] S.-W. Kim, H. Lee, Exact solutions of a charged wormhole, Phys. Rev. D 63 (2001) 064014. doi:[10.1103/PhysRevD.63.064014](https://doi.org/10.1103/PhysRevD.63.064014).
- [31] E. F. Eiroa, G. E. Romero, Linearized Stability of Charged Thin-Shell Wormholes, General Relativity and Gravitation 36 (2004) 651–659. doi:[10.1023/B:GERG.0000016916.79221.24](https://doi.org/10.1023/B:GERG.0000016916.79221.24).
- [32] J. A. González, F. S. Guzmán, O. Sarbach, Instability of charged wormholes supported by a ghost scalar field, Phys. Rev. D 80 (2009) 024023. doi:[10.1103/PhysRevD.80.024023](https://doi.org/10.1103/PhysRevD.80.024023).
- [33] K. Bronnikov, S. Grinek, Conformal continuations and wormhole instability in scalar-tensor gravity, Gravitation & Cosmology 10 (2004).

- [34] J. A. González, F. S. Guzmán, O. Sarbach, Instability of wormholes supported by a ghost scalar field: I. Linear stability analysis, *Classical and Quantum Gravity* 26 (1) (2008) 015010. doi:[10.1088/0264-9381/26/1/015010](https://doi.org/10.1088/0264-9381/26/1/015010).
- [35] M. Sharif, S. Rani, Charged Noncommutative Wormhole Solutions in $f(T)$ Gravity, *European Physical Journal Plus* 129 (2014) 237. doi:[10.1140/epjp/i2014-14237-5](https://doi.org/10.1140/epjp/i2014-14237-5).
- [36] P. H. R. S. Moraes, W. de Paula, R. A. C. Correa, Charged wormholes in $f(R, T)$ -extended theory of gravity, *International Journal of Modern Physics D* 28 (08) (2019) 1950098. doi:[10.1142/S0218271819500986](https://doi.org/10.1142/S0218271819500986).
- [37] T. Harko, Modified gravity with arbitrary coupling between matter and geometry, *Physics Letters B* 669 (5) (2008) 376–379. doi:<https://doi.org/10.1016/j.physletb.2008.10.007>.
- [38] L. V. Jaybhaye, R. Solanki, S. Mandal, P. K. Sahoo, Cosmology in $f(R, L_m)$ gravity, *Physics Letters B* 831 (2022) 137148. doi:[10.1016/j.physletb.2022.137148](https://doi.org/10.1016/j.physletb.2022.137148).
- [39] T. Harko, F. S. Lobo, Generalized Curvature-Matter Couplings in Modified Gravity, *Galaxies* 2 (3) (2014) 410–465. doi:[10.3390/galaxies2030410](https://doi.org/10.3390/galaxies2030410).
- [40] N. M. Garcia, F. S. N. Lobo, Wormhole geometries supported by a nonminimal curvature-matter coupling, *Phys. Rev. D* 82 (2010) 104018. doi:[10.1103/PhysRevD.82.104018](https://doi.org/10.1103/PhysRevD.82.104018).
- [41] T. Harko, F. S. N. Lobo, J. P. Mimoso, D. Pavón, Gravitational induced particle production through a nonminimal curvature-matter coupling, *Eur. Phys. J. C* 75 (2015) 386. doi:[10.1140/epjc/s10052-015-3620-5](https://doi.org/10.1140/epjc/s10052-015-3620-5).
- [42] Y. Sofue, Rotation curve and mass distribution in the galactic center—from black hole to entire galaxy—, *Publications of the Astronomical Society of Japan* 65 (6) (2013) 118.
- [43] S. M. Carroll, *Spacetime and Geometry: An Introduction to General Relativity*, Cambridge University Press, 2019. doi:[10.1017/9781108770385](https://doi.org/10.1017/9781108770385).

- [44] A. Khunt, V. Thomas, P. Vinodkumar, Distinct classes of compact stars based on geometrically deduced equations of state, *International Journal of Modern Physics D* 30 (04) (2021) 2150029. doi:<https://doi.org/10.1142/S0218271821500292>.
- [45] A. Khunt, V. Thomas, P. Vinodkumar, Relativistic stellar modeling with perfect fluid core and anisotropic envelope fluid, *Indian Journal of Physics* 97 (12) (2023) 3379–3393. doi:<https://doi.org/10.1007/s12648-023-02692-1>.
- [46] F. Douchin, P. Haensel, A unified equation of state of dense matter and neutron star structure, *Astronomy & Astrophysics* 380 (1) (2001) 151–167. doi:<https://doi.org/10.1051/0004-6361:20011402>.
- [47] J. Zdunik, Strange stars-linear approximation of the EOS and maximum QPO frequency, arXiv preprint astro-ph/0004375 (2000).
- [48] R. Solanki, Z. Hassan, P. Sahoo, Wormhole solutions in $f(R, L_m)$ gravity, *Chinese Journal of Physics* 85 (2023) 74–88. doi:<https://doi.org/10.1016/j.cjph.2023.06.005>.
- [49] M. S. Morris, K. S. Thorne, U. Yurtsever, Wormholes, time machines, and the weak energy condition, *Physical Review Letters* 61 (13) (1988) 1446. doi:<https://doi.org/10.1103/PhysRevLett.61.1446>.
- [50] J. Wang, K. Liao, Energy conditions in $f(R, L_m)$ gravity, *Classical and Quantum Gravity* 29 (21) (2012) 215016. doi:[10.1088/0264-9381/29/21/215016](https://doi.org/10.1088/0264-9381/29/21/215016).